The Journal of Chemical Physics

# Enhancing the signal strength of surface sensitive 2D IR spectroscopy

Cite as: J. Chem. Phys. **150**, 024707 (2019); https://doi.org/10.1063/1.5065511
Submitted: 10 October 2018 . Accepted: 20 December 2018 . Published Online: 14 January 2019

Megan K. Petti, Joshua S. Ostrander, Vivek Saraswat, Erin R. Birdsall, Kacie L. Rich, Justin P. Lomont, Michael S. Arnold, and Martin T. Zanni



The Journal of Chemical Physics ARTICLE scitation.org/journal/jcp

# Enhancing the signal strength of surface sensitive 2D IR spectroscopy

Cite as: J. Chem. Phys. 150, 024707 (2019); doi: 10.1063/1.5065511
Submitted: 10 October 2018 • Accepted: 20 December 2018 •
Published Online: 14 January 2019



Megan K. Petti,[1,a] Joshua S. Ostrander,[1,a] Vivek Saraswat,[2] Erin R. Birdsall,[1] Kacie L. Rich,[1] Justin P. Lomont,[1] Michael S. Arnold,[2] and Martin T. Zanni[1]

## AFFILIATIONS

[1] Department of Chemistry, University of Wisconsin-Madison, Madison, Wisconsin 53706, USA
[2] Department of Materials Science and Engineering, University of Wisconsin-Madison, Madison, Wisconsin 53706, USA

[a] M. K. Petti and J. S. Ostrander contributed equally to this work.
**Note:** This article is part of the Special Topic "Nonlinear spectroscopy and interfacial structure and dynamics" in J. Chem. Phys.

## ABSTRACT

Spectroscopic techniques that are capable of measuring surfaces and interfaces must overcome two technical challenges: one, the low coverage of molecules at the surface, and two, discerning between signals from the bulk and surface. We present surface enhanced attenuated reflection 2D infrared (SEAR 2D IR) spectroscopy, a method that combines localized surface plasmons with a reflection pump-probe geometry to achieve monolayer sensitivity. The method is demonstrated at 6 $\mu$m with the amide I band of a model peptide, a cysteine terminated $\alpha$-helical peptide tethered to a gold surface. Using SEAR 2D IR spectroscopy, the signal from this sample is enhanced 20 000-times over a monolayer on a dielectric surface. Like attenuated total reflection IR spectroscopy, SEAR 2D IR spectroscopy can be applied to strongly absorbing solvents. We demonstrated this capability by solvating a peptide monolayer with $H_2O$, which cannot normally be used when measuring the amide I band. SEAR 2D IR spectroscopy will be advantageous for studying chemical reactions at electrochemical surfaces, interfacial charge transfer in photovoltaics, and structural changes of transmembrane proteins in lipid membranes.



## I. INTRODUCTION

Interfacial molecular structure and dynamics play an integral role in chemistry, materials science, and biology. From charge transfer in solar cells, to the structural dynamics of voltage-gated ion channels, elucidating the structure of molecules at an interface is central to understanding their function. However, the molecular details of surface chemistry are often lost because most techniques measure signals that are dominated by the bulk response or do not have the sensitivity to measure the small number of molecules present at the surface. For this reason, there has been significant effort to develop techniques that have sufficient signal-to-noise to measure monolayer or sub-monolayer systems.

Vibrational spectroscopy is a widely used tool for studying the molecular structure in the bulk as well as at surfaces. Such one-dimensional techniques include Infrared Reflection Absorption spectroscopy,[1–4] Attenuated Total Reflection (ATR) spectroscopy,[5–7] and Sum Frequency Generation spectroscopy.[8–13] More recently, multiple efforts have been made to extend the monolayer sensitivity of these techniques to vibrational spectroscopies of higher dimensionality.[14–16] Two-dimensional infrared (2D IR) and other multidimensional spectroscopies contain additional features that are not accessible to one-dimensional spectroscopy, such as cross-peaks between coupled oscillators and the ability to experimentally separate the inhomogeneous and homogenous contributions to the linewidth.[17–20] These spectra provide rich information on the structure and dynamics of a sample and have proven to be useful in studying bulk systems in both biology and materials science.[21,22]

The application of two-dimensional vibrational spectroscopy to surfaces and interfaces is difficult due to the small

number of molecules present. The optical density (OD) of a molecular monolayer is easily 1000-times smaller than the typical OD that is often used in a bulk solution sample. Thus, for 2D IR spectroscopy to measure a monolayer, a 1000-time enhancement of the signal is necessary.

The ways to achieve this enhancement are apparent in the mathematical formulism of the third order signal. In general, two-dimensional spectroscopy most often measures the third-order polarization, which in the time domain can be written as[17–20]

$$E^{(3)}_{sig}(t_3,t_2,t_1) \propto P^{(3)}(t_3,t_2,t_1), \tag{1}$$

$$P^{(3)}(t_3,t_2,t_1) \propto \int_0^\infty dt_3 \int_0^\infty dt_2 \int_0^\infty dt_1 E_3(t-t_3)E_2(t-t_3-t_2) \times E_1(t-t_3-t_2-t_1)R^{(3)}(t_3,t_2,t_1), \tag{2}$$

where $E_1(t-t_3-t_2-t_1)$, $E_2(t-t_3-t_2)$, and $E_3(t-t_3)$ are the electric fields of the three incident light pulses, $R^{(3)}(t_3,t_2,t_1)$ is the third-order response function, $P^{(3)}(t_3,t_2,t_1)$ is the third-order polarization, and $E^{(3)}_{sig}(t_3,t_2,t_1)$ is the emitted third-order signal field. The variables, $t_3$, $t_2$, $t_1$, are relative times (compared to real time, $t$) and correspond to the time in between laser pulses. This emitted field is then heterodyned with a local oscillator to give the measured signal[17–20]

$$\begin{aligned} S(t_{LO};t_2,t_1) &\propto \int_0^\infty \left|E_{LO}(t_3-t_{LO}) + E^{(3)}_{sig}(t_3,t_2,t_1)\right|^2 dt_3 \\ &\approx |E_{LO}(t_3-t_{LO})|^2 + \left|E^{(3)}_{sig}(t_3,t_2,t_1)\right|^2 \\ &\quad + 2E_{LO}(t_3-t_{LO})E^{(3)}_{sig}(t_3,t_2,t_1), \end{aligned} \tag{3}$$

where $2E_{LO}(t_3-t_{LO})E_{sig}(t_3,t_2,t_1)$ is the heterodyned signal of interest. To isolate this term, which contains the desired phase information, we subtract off the local oscillator intensity, $|E_{LO}(t_3-t_{LO})|^2$, and ignore the contribution from the emitted field intensity, $\left|E^{(3)}_{sig}(t_3,t_2,t_1)\right|^2$, as it is much smaller than the former term. In practice, this is done by modulating the amplitude of the pump or by phase cycling.[23] The absorptive signal ($-\Delta OD$) is then calculated. To the first order, the absorptive signal is[17–20]

$$-\Delta OD = \log\left(\frac{pump-on}{pump-off}\right) = \log\left(\frac{|E_{LO}(t_3-t_{LO})|^2 + \left|E^{(3)}_{sig}(t_3,t_2,t_1)\right|^2 + 2E_{LO}(t_3-t_{LO})E^{(3)}_{sig}(t_3,t_2,t_1)}{|E_{LO}(t_3-t_{LO})|^2}\right) \approx \frac{2E_{LO}(t_3-t_{LO})E^{(3)}_{sig}(t_3,t_2,t_1)}{|E_{LO}(t_3-t_{LO})|^2}. \tag{4}$$

In this manuscript, we plot the absorptive signal ($-\Delta OD$) as positive, corresponding to a positive bleach of the ground state vibrational modes. From Eq. (4), it is evident that there are two ways to enhance the signal. One can are either increase $E^{(3)}_{sig}(t_3,t_2,t_1)$ or one can decrease $|E_{LO}(t_3-t_{LO})|^2$, so long as $E^{(3)}_{sig}(t_3,t_2,t_1)$ is not altered.

One approach that increases $E^{(3)}_{sig}(t_3,t_2,t_1)$ while simultaneously creating surface sensitivity is a 2D IR spectroscopy variant of attenuated total reflection (ATR). In previous work, Hamm and co-workers use non-resonant plasmonic surface enhancement to increase the third-order signal.[24–26] Others have used gold nano-antennas to obtain even larger signals through on-resonant enhancement, albeit not in an ATR geometry.[27–29] In Hamm's surface enhanced 2D ATR IR spectroscopy, a nanostructured layer of gold coats the surface of a prism that acts as one face of the sample cell. These gold nanostructures have a maximum plasmon absorption in the visible region that extends into the mid-IR. The pump and probe beams of a 2D IR spectroscopy pulse sequence travel through the prism, coming through to the back side of the gold at an angle slightly larger than what is required for total internal reflection. The evanescent waves of the pulses are enhanced by the plasmonic resonance of the gold, which are subsequently absorbed by the molecules near the surface. Hamm has reported plasmonic enhancements that increase the signal size 10-1000 times for monolayers of metal–carbonyl molecules and small molecules with nitrile functional groups.[24–26] The enhancement is dependent on the polarization of light and the localization of the electric field around rough edges or islands on the surface.[24,25] The electric field strength can be so large that vibrational ladder climbing occurs.[25] The ATR design can be used with a flow cell and strongly absorbing solvents, unlike transmission experiments that typically require $D_2O$ or other solvents with little mid-IR absorption.

To provide enhancement by decreasing $|E_{LO}(t_3-t_{LO})|^2$, one can use a four-wave mixing geometry, where the local oscillator is independent from the pump and probe beams. Alternatively, one can use a pump-probe geometry and control the polarization of the emitted signal field relative to the polarization of the probe to provide signal enhancement.[30,31] More recently, in a method developed by Fayer and coworkers, the reflection at an interface is used to decrease the intensity of the local oscillator in a pump-probe geometry.[32,33] In their experiments, a probe beam impinges on the surface of a sample at an angle near Brewster's angle for that air/liquid or air/solid interface so that only a small percentage

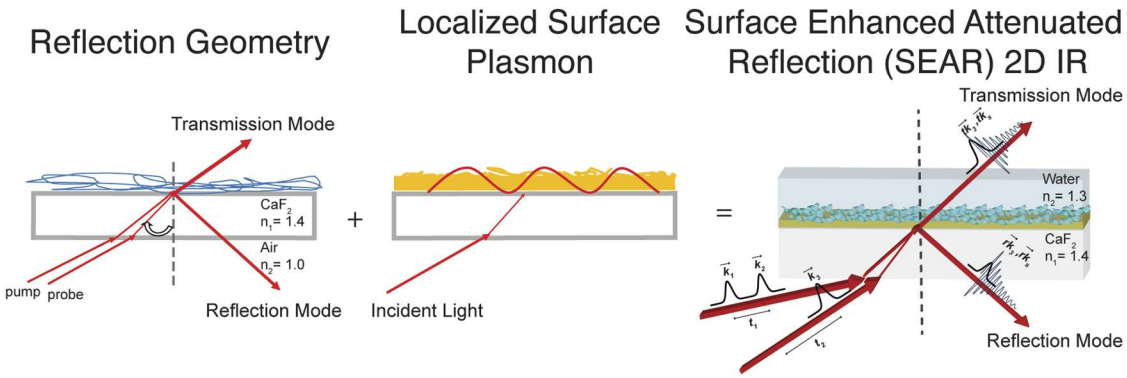


**FIG. 1**. Schematic representation of how surface enhanced attenuated reflection (SEAR) 2D IR spectroscopy combines enhancement mechanisms to create a surface sensitive technique.

of the probe is reflected. Instead of measuring the transmitted probe, as usually done in 2D IR spectroscopy, the reflected probe is collected instead. The monolayer of molecules emits a free induction decay in all directions, but because there is less probe light in the reflected direction, the ratio of the emitted signal field to the probe intensity is larger, via Eq. (4). Like the methods mentioned above, the measured reflected $|E_{LO}(t_3 - t_{LO})|^2$ is independent from the incident $E_3(t - t_3)$ field, allowing $E^{(3)}_{sig}(t_3, t_2, t_1)$ to be maximized as described in Eqs. (1) and (2), respectively. As a result, the $\Delta OD$ is enhanced as the third-order signal strength is independent from the measured attenuated local oscillator that is reflected from the surface. This reflection enhanced 2D IR spectroscopy has been applied to interfaces where the probe beam impinges on the sample from the air so that there is a large change in the index of refraction, creating a relatively large Brewster's angle. Nishida *et al.* reported signal enhancement of 50-times.[32] While this enhancement is not as large as plasmon enhanced 2D IR,[24–29] it is applicable to solution surfaces where interesting phenomena using metal carbonyl molecules has been observed.[33]

In this article, we report a variation of 2D IR spectroscopy that combines the approaches of Fayer and Hamm (Fig. 1). We measure a reflected probe beam like Fayer and co-workers, but we invert the sample geometry so that the first interface impinges from the back of our sample cell. In the inverted geometry, the probe light travels from an interface of higher refractive index (in this case $CaF_2$), to lower refractive index (air or water). In standard ATR, the beams impinge at the critical angle. Here, the critical angle is purposely avoided to decrease the local oscillator intensity, consequently any sample window can be used, limiting dispersion introduced by ATR prisms. The inverted reflection geometry allows for the use of strongly absorbing solvents as well as flow cells. Following Hamm and co-workers, we coat the sample cell window with nanostructured gold to induce localized surface plasmons. The combination of these two sources of enhancement, localized surface plasmon and reflection geometry, create a method we call surface enhanced attenuated reflection (SEAR) 2D IR spectroscopy. These mechanisms allow the $\Delta OD$ to be enhanced by increasing the generated third-order signal, while decreasing the intensity of the local oscillator. We have measured enhancements of 190-20 000 times. We demonstrate SEAR 2D IR spectroscopy by measuring at 6 $\mu$m the amide I mode on a monolayer of peptides in both $D_2O$ and $H_2O$ solvents.

## II. METHODS

### A. Laser system

A regenerative amplifier (Coherent Libra) with an output of 3.4 W, 50 fs, centered at 800 nm pumps a commercial optical parametric amplifier (OPA) (TOPAS, Light Conversion). The signal and idler pulses are then mixed collinearly in a $AgGaS_2$ difference frequency generation (DFG) crystal to generate mid-IR light with a center wavelength of 6 $\mu$m. The mid-IR pulses have a duration of <100 fs with pulse energies around 18-20 $\mu$J. The mid-IR output is sent through a 90/10 $CaF_2$ beam splitter to create the pump and probe lines. The pump pulse is shaped by using a germanium acousto-optical modulator (Ge-AOM) pulse shaper as previously described.[23,34,35] Both probe and pump pulses are polarized to either s- or p-polarization by using half wave plates and polarizers.

The pump and probe pulses are spatially and temporally overlapped at the sample and are focused using 7.5 cm focal length gold parabolic mirrors. For the reflection geometry, the sample is rotated perpendicular to the table. The back-substrate interface is the first interface the mid-IR light hits. The reflected signal is collimated using a convex lens before being directed to a 32-pixel MCT array.

### B. Sample preparation

*CORM-3 Thin film*: Carbon monoxide releasing molecule 3 (CORM-3) was purchased from Sigma-Aldrich. A 2 mg/ml solution of CORM-3 was made in chloroform. Thin film samples were made by slowly drying the CORM-3 solution on a $CaF_2$ substrate in a nitrogen rich environment. From the linear FTIR spectrum, we estimate the film thickness to be

1-3 nm. *Cys-terminated Ovispirin-1*: Cys-terminated ovispirin-1 (cys-ovispirin-1) was synthesized using a standard fluorenylmethyloxycarbonyl (FMOC) protecting group solid-phase peptide synthesis with a CEM Liberty Blue Automated Peptide Synthesizer, cleaved with trifluoroacetic acid (TFA), and purified using reverse-phase high-performance liquid chromatography (HPLC).[35,36] The purified peptide was made into a 0.02 mM solution in 10% tris buffer (pH = 12.16) and 90% HPLC grade ethanol. Gold films (Au% > 99.99%) with thicknesses of 3 nm were deposited on $CaF_2$ substrates in a thermal evaporator. The deposition rate was 0.1 Å/s at a vacuum of $8 \times 10^{-7}$ torr. The thickness was monitored via a quartz crystal microbalance. Determination of the plasmon frequency was found with a UV-Vis spectrometer (Fig. S1). The Au/$CaF_2$ substrate was submerged in the cys-ovispirin-1 solution for 12 h to form a monolayer. The sample was gently rinsed with HPLC grade ethanol and dried under nitrogen for subsequent measurement. For the hydrated sample, either $D_2O$ or deionized $H_2O$ was added on top of the monolayer.

## III. RESULTS

In the following, we first quantify the enhancement of reflection enhanced 2D IR spectroscopy employed in an inverted geometry using a strongly absorbing metal carbonyl system. Second, we thermally evaporate gold onto a $CaF_2$ window and measure the resulting plasmonic enhancement in a standard transmission geometry for a monolayer of peptides. Third, we measure the additional improvement in the signal by measuring the peptide sample in a reflection, rather than transmission, geometry. Finally, we hydrate the peptides with $D_2O$ and $H_2O$ to demonstrate the utility of the method for measuring monolayers of peptides in strongly absorbing solvent.

### A. Signal enhancements of a metal carbonyl thin film on a dielectric surface using an inverted reflection pump-probe geometry

Shown in Fig. 2 are the 2D IR spectra of carbon monoxide releasing molecule 3 (CORM-3) drop-cast onto a 2 mm $CaF_2$ window to make a thin film. The opticaldensity of the film is approximately 10 mOD. While CORM-3 has 3 metal carbonyl functional groups, one of the axial carbonyls becomes a carboxylic acid group in the inactive state.[37,38] CORM-3 has previously been used as a precursor to label proteins to study protein-water interfaces.[39] In Fig. 2(a), a 2D IR spectrum is shown of the CORM-3 film using a standard transmission pump-probe geometry in which the pump and probe beams impinge on the sample at 35° to the normal at the $CaF_2$/air interface. Figure 2(a) is the spectrum obtained by collecting the transmitted probe beam. The spectrum contains two sets of diagonal pairs of peaks, at $\omega_{pump}$ = 2060 $cm^{-1}$ and 1980 $cm^{-1}$, which are created by the metal carbonyl modes of CORM-3 in its inactivated form.[38] The bleaches of the ground state vibrational modes appear close to the diagonal and are plotted to have a positive intensity. The peaks are elongated along the diagonal, indicating that the vibrational modes are inhomogeneously broadened. This broadening is expected for thin films and is similar to ions previously studied in a glass[40] and other films of metal carbonyls.[41–43]

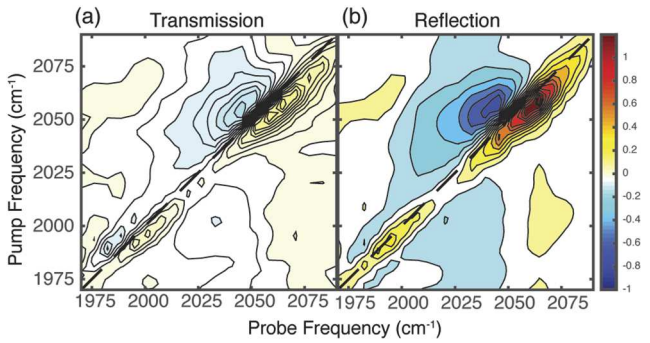


**FIG. 2**. CORM-3 thin film spectra collected in (a) transmission and (b) inverted reflection geometries. The pump and probe beams are p-polarized and the spectra are plotted on the same normalized color map.

Shown in Fig. 2(b) is the CORM-3 thin film sample measured in an inverted-reflection pump-probe geometry. The same beam geometry and angle of incidence is used as before, but rather than measuring the portion of the probe that is transmitted through the thin film, the small portion of probe light reflected off the interface between the $CaF_2$ and the film of CORM-3 is measured. The amount of reflected light from the interface depends on the polarization of light used and the incident angle. Here, p-polarized pump and probe beams were used. The p-polarized probe beam travels from $CaF_2$, a higher refractive index (n = 1.4) material, to air, a lower refractive index (n = 1.0) material, at an incident angle of 35° at the $CaF_2$/air interface, causing less than 1% of the probe beam to be reflected. The raw data is collected as a change in optical density (ΔOD). This ΔOD is normalized to the reflection experiment and depicted in Fig. 2. We measure a 40-times enhancement in the reflection over the transmission 2D IR spectrum, consistent with measurements of Fayer and co-workers on similar samples. Thus, an inverted-reflection pump-probe geometry, i.e., coming back from the back of the sample, provides the expected enhancement for a reflection geometry.

### B. Surface plasmon enhancement of a peptide monolayer on a rough nanometer thin Au/$CaF_2$ substrate

Having observed signal enhancement with the inverted reflection geometry comparable to what was reported by Fayer and co-workers,[32] we now investigate the use of localized surface plasmons, like what has been used with Hamm and co-worker's 2D ATR IR method.[25,26] We apply this approach to measure the amide I mode of a polypeptide monolayer, requiring 6 $\mu$m mid-IR light. The amide I mode probes the protein backbone and the resulting peak frequencies provide information on the secondary structure of the peptide.[21,44,45] The measured peptide, ovispirin-1, is an antimicrobial amphipathic peptide consisting of 18 residues. Based on high-resolution nuclear magnetic resonance (NMR)

experiments, it forms an $\alpha$-helix from residues 4–16 in helix-promoting solvents of 33% 2,2,2-trifluoroethanol/67% phosphate buffer solution at pH 6.5.[46] Due to its amphipathic nature, it also forms an $\alpha$-helix on lipid bilayers[47] as well as polystyrene surfaces[48] with a kink at residue 14 according to solid-state NMR[49] and 2D IR spectroscopy studies.[47] Here, a cysteine residue was added to the C-terminus to form a monolayer on a gold surface through a cysteine thiol-gold bond.[50,51] This functionalized 19-residue peptide will be referred to as cys-ovispirin-1. As described in Sec. II, gold was deposited onto a $CaF_2$ substrate using thermal-evaporation to a thickness of 3 nm. Gold films deposited in this way and at this thickness are rough and contain nanostructures that can support mid-IR nonresonant localized surface plasmon enhancement.[25,26,52]

To explore the enhancement caused by localized surface plasmons, we first use transmission pump-probe 2D IR spectroscopy. Figure 3(a) is a transmission 2D IR spectrum of a dried monolayer of cys-ovispirin-1 on 3 nm Au/$CaF_2$. The spectrum contains a diagonal pair of peaks at $\omega_{pump}$ = 1653 $cm^{-1}$ as well as a peak at $\omega_{pump}$ = 1634 $cm^{-1}$. Figure 3(b) shows the transmission 2D IR spectrum of the same sample, except in a $D_2O$ hydrated environment. As in the dried sample, a diagonal pair of peaks at $\omega_{pump}$ = 1653 $cm^{-1}$ is observed, as well as a peak at $\omega_{pump}$ = 1634 $cm^{-1}$. A third peak is observed in the $D_2O$ hydrated peptide at $\omega_{pump}$ = 1621 $cm^{-1}$ and a small cross-peak is observed between the two lower frequency modes.

Based on prior work,[48] in our spectra of cys-ovispirin-1, we attribute the higher frequency peak at 1653 $cm^{-1}$ to α-helical components, while we assign the lower frequency peak at 1634 $cm^{-1}$ to random coil contributions of cys-ovispirin-1. From the intensities of these peaks, we conclude that cys-ovispirin-1 has a partial α-helical structure when bound to the gold surface in both dehydrated and hydrated environments, although we do not attempt to quantify the structural distribution as it is not necessary for the purposes of this manuscript. The conservation of both diagonal peaks between the dried and hydrated cys-ovispirin-1 monolayers [Figs. 3(a) and 3(b)] is evidence that the signal is from proteins only at the surface and not from the bulk (Fig. S2). We attribute the third peak in the $D_2O$ hydrated spectrum at $\omega_{pump}$ = 1621 $cm^{-1}$ to different hydrogen bonding environments of the peptide backbone, as some residues may be facing the hydrophobic Au surface, while others are fully hydrated with $D_2O$.[53–57]

To quantify the enhancement created by the localized surface plasmon, we take an approach first outlined by Grechko and Zanni[58–60] and then adopted for signal enhancement calculations by Donaldson and Hamm[24] The enhancement is found by determining the relative transition dipole strength as described in Eq. (5). The linear absorption signal is proportional to the concentration, c, and the transition dipole strength, $|\mu|^2$, while the heterodyned 2D IR signal is proportional to $c \times |\mu|^4$. Taking the ratio of the linear and nonlinear signals with respect to a calibrant allows for the transition dipole strength of the molecule of interest to be found independent of concentration and instrument parameters. In this case, N-methylacetamide (NMA) in chloroform was used as a calibrant because it absorbs at nearly the same frequency as the surface-bound peptide.[55,56] The calibrant is needed to account for any discrepancies in the laser fluence or spatial overlap of the pump and probe pulses for the 2D IR experiment[61]

$$|\mu|^2_{sample} = \frac{|\mu|^2_{calibrant}\left(S^{2D\ IR}_{sample}/A^{IR}_{sample}\right)}{\left(S^{2D\ IR}_{calibrant}/A^{IR}_{calibrant}\right)} = \frac{|\mu|^2_{calibrant}\left(\Delta OD_{sample}/OD_{sample}\right)}{\left(\Delta OD_{calibrant}/OD_{calibrant}\right)}, \quad (5)$$

$$\frac{|\mu|^2_{monolayer}}{|\mu|^2_{bulk}} = Enhancement\ Factor, \quad (6)$$

$$2D\ Signal\ Enhancement = (Enhancement\ Factor)^2 = \frac{|\mu|^4_{monolayer}}{|\mu|^4_{bulk}}. \quad (7)$$

In Eq. (5), $\Delta OD_{sample}$ and $\Delta OD_{calibrant}$ are the 2D signal intensities for the cys-ovispirin-1 monolayer and NMA solution, respectively, and $OD_{sample}$ and $OD_{calibrant}$ are the FTIR signal intensities. To find the enhancement factor from the surface plasmon, the ratio of the transition dipole strength of

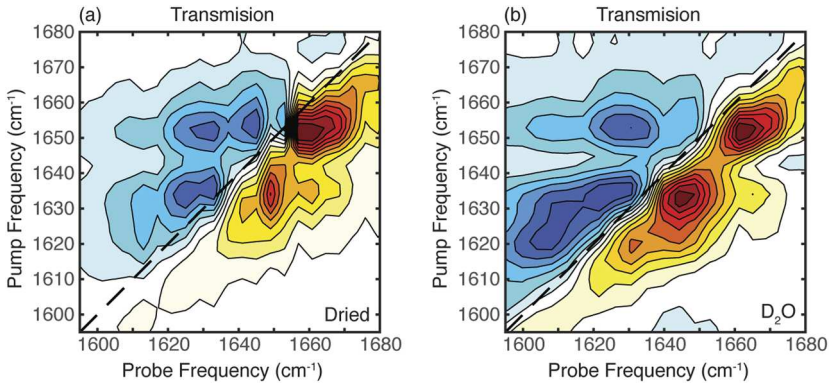


**FIG. 3.** (a) Transmission spectrum of dried cys-ovispirin-1 on 3 nm Au/$CaF_2$. (b) Transmission spectrum of cys-ovispirin-1 on 3 nm Au/$CaF_2$ hydrated with $D_2O$. S-polarized pump and probe beams were used for both spectra.

**TABLE I**. Calculated localized surface plasmon enhancement for 2D IR signals based on measurements of the effective transition dipole strength.

| Sample | $\|\mu\|^2$ effective ($D^2$) Random coil | α-helix | Enhancement factor | 2D signal enhancement |
|---|---|---|---|---|
| Cys-ovispirin-1 on 3 nm $Au/CaF_2$, dry | 0.92 | 18.8 | 7.69–78.3 | 59.1–6140 |
| Cys-ovispirin-1 on 3 nm $Au/CaF_2$, hydrated with $D_2O$ | 1.48 | 2.81 | 11.7–12.4 | 137–153 |

the monolayer and bulk is taken [Eq. (5)]. Bulk cys-ovispirin-1 in buffer adopts an α-helix conformation (Fig. S2). However, based on the spectra in Fig. 3, we know that the peptide monolayer does not adopt a completely α-helical conformation, but also contains random coil structure. Thus, the bulk transition dipole strength of the peptide sample with the same conformation as that of the monolayer is not known. To account for this variable, we report a range of enhancement factors based on the two secondary structures observed in the peptide monolayer spectra. A previous study has determined the transition dipole strength of an α-helix to be 0.24 $D^2$, while a random coil conformation has a transition dipole strength of 0.12 $D^2$.[58] We use these values when calculating the enhancement factors.

The enhancement factor squared is the effective 2D signal enhancement due to the scaling of the transition dipole strength in the nonlinear absorption signal [Eq. (7)]. We again report a range based on the enhancement factors found for the two secondary structures observed in the peptide monolayer. The reported enhancement factors and 2D signal enhancement (Table I) are qualitatively similar to what has been reported previously for linear infrared absorption spectroscopy[62–64] and 2D IR spectroscopy.[24–26]

### C. SEAR 2D IR spectroscopy of a peptide monolayer in a strongly absorbing solvent

With the enhancements from the inverted reflection geometry and localized surface plasmon quantified, we now

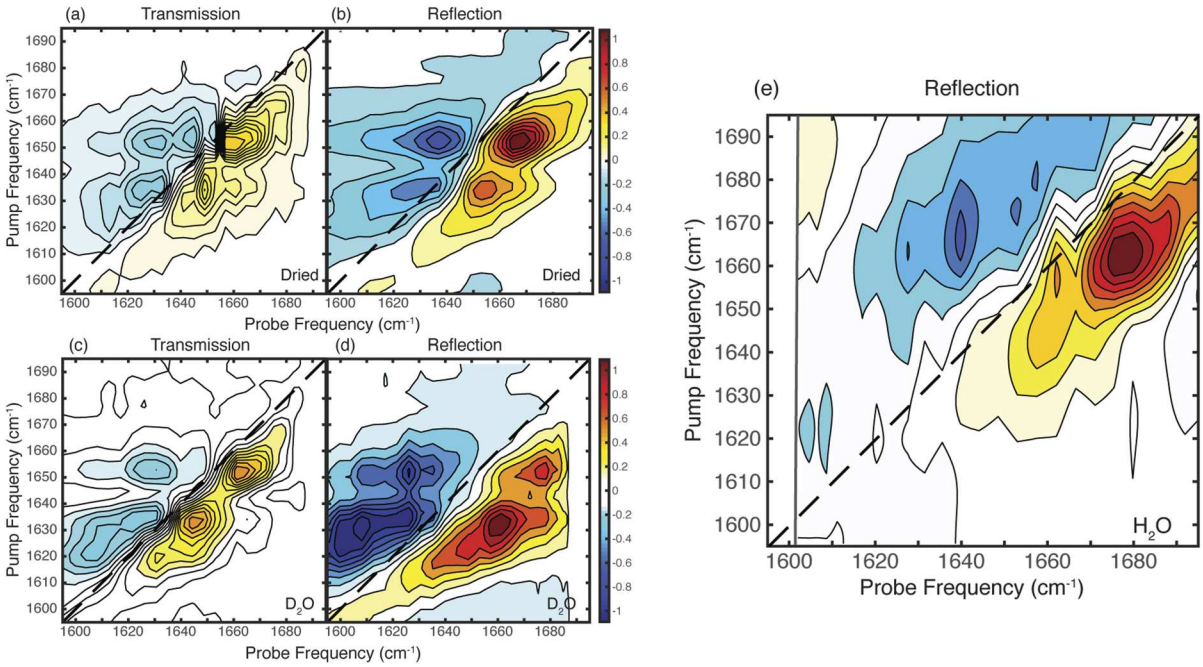


**FIG. 4**. Dried monolayer of cys-ovispirin-1 on 3 nm $Au/CaF_2$ 2D IR spectra taken in a (a) transmission geometry and with (b) SEAR 2D IR spectroscopy plotted on the same normalized color map. Monolayer of cys-ovispirin-1 on 3 nm $Au/CaF_2$ hydrated with $D_2O$ 2D IR spectra taken in a (c) transmission geometry and with (d) SEAR 2D IR spectroscopy plotted on the same normalized color map. (e) Monolayer of cys-ovispirin-1 on 3 nm $Au/CaF_2$ hydrated with $H_2O$ spectrum taken with SEAR 2D IR spectroscopy. The vertical grey line indicates the last pixel of the MCT detector. Consequently, frequencies lower than ~1600 $cm^{-1}$ are not detected. A s-polarized pump and probe were used for all the spectra shown here.

use SEAR 2D IR spectroscopy to measure two peptide monolayer samples. One sample is dried cys-ovispirin-1 on 3 nm Au/$CaF_2$, and the second sample is $D_2O$ hydrated cys-ovispirin-1 on 3 nm Au/$CaF_2$. The two spectra are shown in Figs. 4(b) and 4(d), respectively. These SEAR 2D IR spectra are obtained with an angle of incidence of 32° from the normal of the air/$CaF_2$ interface. This external incident angle at the air/$CaF_2$ interface corresponds to an internal incident angle of 22° at the $CaF_2$/sample interface, and it is the reflection from this internal interface that is measured. For the two samples measured, both the pump and probe beams were set to s-polarized. For comparison, the transmission 2D IR spectra of the dried and hydrated monolayer samples of cys-ovispirin-1 on 3 nm Au/$CaF_2$ from Figs. 3(b) and 3(c) are replotted in Figs. 4(a) and 4(c), respectively. The z-axis of Figs. 4(a) and 4(c) are scaled to that of Figs. 4(b) and 4(d). When comparing, the two spectra for the dried sample [Figs. 4(a) and 4(b)], the 1653 $cm^{-1}$ peak and 1634 $cm^{-1}$ peak are retained, as well as the inhomogeneous line shape. For the $D_2O$ hydrated sample [Figs. 4(c) and 4(d)], again the frequency of the three peaks are retained (1653 $cm^{-1}$, 1634 $cm^{-1}$, and 1621 $cm^{-1}$). The reflection geometry provides additional enhancements of 3.2- and 2.5-times in Figs. 4(b) and 4(d) over the transmission geometry. These enhancements, while smaller than in Fig. 2, still reduces the data collection time, as explained in Sec. IV.

Figure 4(e) is a SEAR 2D IR spectrum of cys-ovispirin-1 on 3 nm Au/$CaF_2$ hydrated with $H_2O$. The amide I band of peptides and proteins are usually measured in $D_2O$ when using IR spectroscopy because the bending vibrational mode of $H_2O$ absorbs in this same region,[65] prohibiting samples with a reasonable path-length. With SEAR 2D IR spectroscopy, water absorption is minimized since the reflected probe beam does not penetrate deeply into the solvent and the emitted field is generated close to the surface.[32] We note that the SEAR 2D IR spectrum of cys-ovispirin-1 on 3 nm Au/$CaF_2$ hydrated with $H_2O$ has two features like in the $D_2O$ spectra, but these peaks are blue shifted by ~8 $cm^{-1}$ and the ratio of intensities are different. In $H_2O$, there is one very intense peak at $\omega_{pump}$ = 1661 $cm^{-1}$, and one less intense peak at $\omega_{pump}$ = 1642 $cm^{-1}$. We discuss these differences below.

## IV. DISCUSSION

SEAR 2D IR spectroscopy builds from previous work that allows for surface sensitive 2D IR spectroscopy.[24–29,32,33] Here, the combination of a reflection geometry and localized surface plasmons effectively decreases the local oscillator intensity while also increasing the third-order signal, providing enhancements of the measured ΔOD of the amide I mode of a peptide monolayer. Table II outlines the signal enhancement observed from the localized surface plasmon, the inverted reflection geometry, and the total enhancement of SEAR 2D IR signals for cys-ovispirin-1 on 3 nm Au/$CaF_2$. Since we cannot measure a spectrum of peptides without plasmon enhancement, the total enhancement of SEAR 2D IR spectroscopy is calculated by multiplying together the two sources of enhancement used in the technique. Thus, the overall signal enhancement obtained using SEAR 2D IR spectroscopy is 190-20 000-times (Table II), with most of the enhancement coming from the use of localized surface plasmons. Below, we discuss the mechanism of enhancement for SEAR 2D IR spectroscopy and experimental considerations for this technique. SEAR 2D IR spectroscopy also allows for the use of strongly absorbing solvents and is demonstrated here with a peptide monolayer hydrated with $H_2O$. We report on differences in the amide I mode of a peptide monolayer in $D_2O$ and $H_2O$.

### A. Enhancement mechanisms of SEAR 2D IR

The dominate enhancement factor in SEAR 2D IR spectroscopy comes from the use of localized surface plasmons (Table II). In terms of the 2D IR signal, using localized surface plasmons enhances the generated third-order signal field [Eqs. (1) and (2)], leading to a larger measured ΔOD [Eq. (4)]. Previously, it was found that the enhancement from the localized surface plasmon from the rough gold nanostructures was dependent on the polarization of light.[25,26] Because of the rough structure of the gold used in their study, there were gaps between nanostructures within the plane of the substrate. When using s-polarized light, the localized surface plasmon was polarized within the plane of the surface and confined more tightly in these gaps, making "hot-spots" of high intensity fields that provided 10-100-times greater (depending on the thickness of gold) enhancement then when p-polarized light was used.[25,26] The same confinement effect was not observed for p-polarized light, as the surface plasmon is polarized perpendicular to the surface normal and "hot-spots" are not observed. It should be noted that this enhancement is based on localized surface plasmons and not surface plasmon polaritons, which have different excitation mechanisms.[25,26,66–68] We used s-polarized pump and probe beams to take full advantage of the localized surface plasmon enhancement mechanism. While the non-resonant localized surface plasmon used here provides large enhancement (Table II), more enhancement can be obtained by considering the plasmon frequency. As the plasmon frequency moves closer to resonance with the vibrational modes of interest, the enhancement increases drastically.[28,29] Other plasmonic structures, such as nano-arrays, nano-antennas, or nano-stars may have different plasmon frequencies and polarization dependencies that can be considered to provide more enhancement. Here, the rough nanometer thin Au on $CaF_2$ substrates used have a plasmon frequency in the visible (Fig. S1) that extended into the mid-IR and provides 50-6000-times enhancement (Table II).

While the use of localized surface plasmons increases the third-order signal, the inverted reflection geometry decreases the intensity of the local oscillator. The purely absorptive 2D IR signal measured here is inversely proportional to the intensity of the local oscillator, as described by Eq. (4). Thus, decreasing this background intensity will increase the third-order signal. In a fully non-collinear geometry, this is trivial, as the local oscillator can be independently attenuated without influencing the third-order signal. However, in a partially

**TABLE II**. Enhancements of 2D IR signals from localized surface plasmons, the inverted reflection geometry, and SEAR 2D IR spectroscopy.

| Sample | Localized surface plasmon enhancement | Inverted reflection geometry enhancement | SEAR 2D IR spectroscopy enhancement |
|---|---|---|---|
| Cys-ovispirin-1 on 3 nm Au/$CaF_2$, dried | 59.1–6140 | 3.2 | 190–20 000 |
| Cys-ovispirin-1 on 3 nm Au/$CaF_2$, hydrated with $D_2O$ | 137–153 | 2.5 | 340–380 |

collinear geometry, as used here, the probe pulse acts as the local oscillator, and the generated signal is in the same phase-matched direction as the probe pulse. Fayer and co-workers used the reflection from a surface to control the intensity of the local oscillator in a pump-probe geometry.[32,33] SEAR 2D IR spectroscopy uses this same principle, except in an inverted reflection geometry.

In SEAR 2D IR spectroscopy, two conditions are controlled: the incident angle of the incoming light at the sample and the polarization of light used. The amount of light reflected vs. transmitted at the interface is determined by the refractive indices of the materials that make the interface, the angle of incidence, and the polarization of light. For p-polarized light, the amount of reflected light goes to zero at Brewster's angle. Thus, by setting the incident angle close to Brewster's angle, and using p-polarized light, the amount of reflected local oscillator can be diminished. Alternatively, s-polarized light can be used, which reduces the local oscillator by ~90% for most angles. Either way, the reflected signal field strength ($E^{(3)}_{sig}(t_3, t_2, t_1)$) is maintained and the local oscillator intensity ($|E_{LO}(t - t_3)|^2$) is substantially reduced, resulting in a large signal over a small background.[32,33] To determine the incident angle and the polarization of light to use, it is helpful to calculate the percentage of light reflected from different interfaces.

The Fresnel equations describe this reflectivity and are used to produce the graphs for three different interfaces in Fig. 5. These equations are as follows:

$$R_s\,\% = \left(\frac{n_1\cos(\theta_1) - n_2\cos(\theta_2)}{n_1\cos(\theta_1) + n_2\cos(\theta_2)}\right)^2 \times 100, \tag{8}$$

$$R_p\,\% = \left(\frac{n_1\cos(\theta_2) - n_2\cos(\theta_1)}{n_1\cos(\theta_2) + n_2\cos(\theta_1)}\right)^2 \times 100, \tag{9}$$

where $R_s$% and $R_p$% correspond to the percentage of s- and p-polarized light reflected. $n_1$ and $n_2$ are the refractive indices for the first and second interface, respectively. The refractive indices for the materials used are n = 1 for air, n = 1.4 for $CaF_2$, and n = 1.26 for water. $\theta_1$ is the angle of incidence, while $\theta_2$ is the angle of transmittance. Brewster's angle is where p-polarized light (green in Fig. 5) goes to zero and is defined as

$$\theta_{Brewster's} = \tan^{-1}\left(\frac{n_2}{n_1}\right). \tag{10}$$

For the air/$CaF_2$ interface, Brewster's angle is 54.5,° whereas for the $CaF_2$/air interface, Brewster's angle is the complement angle at 35.5°. With the inverted reflection geometry, less than 3% of p-polarized light and less than 10% of s-polarized light is reflected for all incident angles less than Brewster's angle at the $CaF_2$/air interface. For p-polarized light, this leads to a predicted enhancement of 7-10-times at angles less then Brewster's angle, which then drastically increases as the incident angle moves closer to Brewster's angle, until ultimately diverging (Fig. S3). For s-polarized light, a maximum enhancement of 7-times is expected for incident angles less than Brewster's angle, before going to zero at the critical angle (Fig. S3). Thus, to get a large enhancement, the

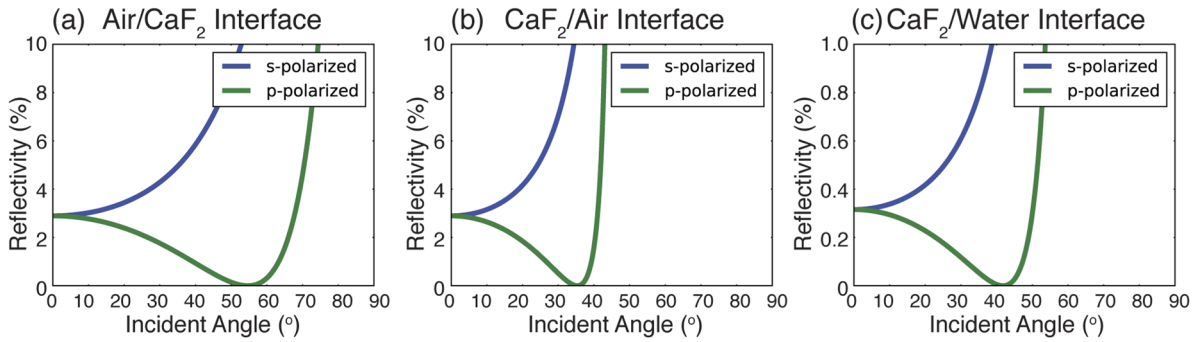


**FIG. 5**. The amount of light reflected (%) as a function of incident angle at (a) air/$CaF_2$, (b) $CaF_2$/air, and (c) $CaF_2$/water interfaces as defined by the Fresnel equations for both s- and p-polarized light.

pump and probe should both be p-polarized and the incident angle should be within 2°–3° of Brewster's angle. Doing so diminishes the amount of reflected light (Fig. 5) by 99%-100% (theoretically) and effectively decreases the local oscillator to increase the measured ΔOD as described in Eq. (4).[32] The enhancement obtained when using an inverted reflection geometry is an order of magnitude less than the enhancement from the localized surface plasmons. For this reason, we capitalized on the localized surface plasmon enhancement and use s-polarized light for the SEAR 2D IR measurement of the peptide monolayer. Doing so results in an enhancement of 3.2-times for the dried monolayer [Fig. 4(b)] and 2.5-times for the $D_2O$ hydrated monolayer [Fig. 4(d)] over the transmission spectra. Compared to the inverted reflection geometry enhancement observed with CORM-3, this enhancement is an order of magnitude less. The difference between the CORM-3 and cys-ovispirin-1 spectral enhancement based on the inverted reflection geometry is that in the latter case, there is 5% more reflected light with the experimental conditions used. Because of this difference in reflection, the local oscillator is not attenuated as much in the cys-ovispirin-1 spectra as in the CORM-3 spectrum, leading to lower reflection enhancements as predicted[32] (Fig. S3) and observed.

Additionally, we would expect that the hydrated cys-ovispirin-1 monolayer would be enhanced more than the dry cys-ovispirin-1 monolayer based on the amount of light reflected from the hydrated interface (Fig. 5). However, we observe similar enhancements (Table II). We attribute this discrepancy to the reflectivity of the nanostructured gold on the $CaF_2$ substrate. This thin layer of gold is reflecting more light than what would be predicted for a $CaF_2$/air or $CaF_2$/water interface, leading to observed enhancements that are less than expected. While these enhancements are smaller than expected, using a reflection geometry does reduce the data collection time. For example, to obtain a transmission spectrum of the dried or $D_2O$ hydrated cys-ovispirin-1 on 3 nm Au/$CaF_2$ with the same signal-to-noise as the SEAR 2D IR measurements taken with s-polarized light, the spectrum would have to be averaged 5-10 times longer. It should also be noted that in the peptide monolayer case, the spectra are also enhanced by the localized surface plasmon. This leads to an overall SEAR 2D IR enhancement of 100-20 000-times (Table II.) and is much larger than what could be obtained by either enhancement technique alone.

In practice, the quality of the spectra that one can gain from SEAR 2D IR spectroscopy, or any method that attenuates the local oscillator, is limited by the shot noise limit of the detector. While attenuating the local oscillator improves the ΔOD, one still needs sufficient local oscillator intensity to be above the detector dark counts. In the case here, s-polarized light was used to maximize the localized surface plasmon enhancement but was also necessary to have sufficient light hit the detector. We estimate that ~40 nJ is reflected at the $CaF_2$/water interface for our samples, which is the limit of detection for our monochromator and detector. By considering the sample interface, both the polarization of light and the incident angle can be selected for an experiment to provide sufficient signal-to-noise.

### B. Measuring a peptide monolayer in a strongly absorbing environment with SEAR 2D IR spectroscopy

In SEAR 2D IR spectroscopy, the signal field is emitted in all directions and the heterodyned signal is measured in the reflection direction. The signal field and probe pulse in this direction do not penetrate the solvent environment. For biological experiments where amide I modes are of interest, this allows for those systems to be measured in $H_2O$. Currently, 2D IR experiments on peptides and proteins in a transmission geometry rely on deuterated solvents. Being able to use $H_2O$ or other strongly absorbing solvent increases the variety of systems that can be measured with 2D IR spectroscopy, such as biological tissues, electrochemical surfaces, and photovoltaic devices. We demonstrate this capability by measuring a peptide monolayer hydrated with $H_2O$.

The SEAR 2D IR spectrum of cys-ovispirin-1 on 3 nm Au/$CaF_2$ hydrated with $H_2O$ has two diagonal peaks associated with α-helical and random coil secondary structure contributions [Fig. 4(e)]. The spectrum of cys-ovispirin-1 on 3 nm Au/$CaF_2$ hydrated with $D_2O$ also has two sets of peaks [Fig. 4(d)]. The main differences in these two spectra are the frequency at which the α-helical and random coil amide I peaks absorb, and the relative intensity of these two peaks. There are two factors that contribute to these differences: the transition dipole strength and hydrogen/deuterium (H/D) exchange.

Regarding the former, the amide I mode consists of 85% C=O stretch, 10% C—N stretch, and 5% N—H in-plane bending.[69] When the N—H is changed to a N—D, the amide vibrational mode is altered. This change is validated by calculating the carbonyl vibrational frequency and intensity of N-methylacetamide (NMA) and deuterated N-methylacetamide (d-NMA). A B3LYP functional and cc-pvtz basis was used and found that for NMA, the amide I vibrational frequency is 1697.039 $cm^{-1}$, while for d-NMA, the frequency is red shifted to 1681.673 $cm^{-1}$. The transition dipole strength of the d-NMA carbonyl frequency is $|\mu|^2$ = 0.150 $D^2$ or 1.07-times more than NMA (Fig. S5). 2D IR signals are proportional to $|\mu|^4$,meaning that the d-NMA carbonyl vibrational mode will be 1.14-times more intense in the 2D IR measurement. Thus, deuterating the nitrogen of the amide I modes increases the intensity over non-deuterated amide I modes.

Regarding the latter, different peptide conformations undergo H/D exchange at different rates. For random coil structures, H/D exchange happens on the milliseconds to seconds time scale, while β-sheets and α-helices take anywhere from a few minutes to hours to completely exchange.[70,71] In our experiments, spectra were collected immediately after solvation, so only the random coil regions will be fully exchanged. When hydrated with $H_2O$, the peptide monolayer spectrum resulted in a more intense α-helix peak at $\omega_{pump}$ = 1661 $cm^{-1}$ and a less intense random coil peak at $\omega_{pump}$ = 1642 $cm^{-1}$. The peptide monolayer was then dried and

hydrated with $D_2O$, and the resulting SEAR 2D IR spectrum has an α-helix peak at $\omega_{pump}$ = 1653 $cm^{-1}$ and a random coil peak at $\omega_{pump}$ = 1634 $cm^{-1}$. Thus, both amide I peaks frequencies have redshifted as expected.[72] The random coil peak has also increased in relative intensity compared to the α-helix and is consistent with incomplete H/D exchange of the α-helix. Therefore, our data is consistent with full H/D exchange of the random coil peptide secondary structure and partial exchange of the α-helix.

## V. CONCLUSIONS

SEAR 2D IR spectroscopy combines two techniques that each provide different mechanisms to achieve signal enhancement and monolayer sensitivity. Previously, Fayer and co-workers have established a reflection enhanced 2D IR spectroscopy in a pump-probe geometry, while the use of localized surface plasmons for surface enhanced 2D ATR IR has been pioneered by Hamm and co-workers. A reflection geometry allows the local oscillator to be attenuated independently and maintain the maximum $E^{(3)}_{sig}(t_3, t_2, t_1)$ strength, analogous to fully collinear geometries and polarization methods. The use of localized surface plasmons increases the $E^{(3)}_{sig}(t_3, t_2, t_1)$ field strength of molecules on the surface. Taken together, these techniques lower the intensity of the local oscillator in a pump-probe geometry and increase the third-order signal field strength of the measurement. Mathematically, this decreases the denominator and increases the numerator that define the ΔOD measured, optimizing the way that signal enhancement can be achieved. In Secs. III–IV, the individual enhancement of the two approaches used and the overall enhancement of SEAR 2D IR spectroscopy were demonstrated and quantified. We report an enhancement of 20 000-times. SEAR 2D IR spectroscopy was applied to the surface bound peptide ovispirin-1 in both dehydrated and hydrated environments. With SEAR 2D IR spectroscopy, the spectrum of a monolayer of peptide was obtained in $H_2O$, a strongly absorbing solvent.

These proof of principle experiments presented here establish more general criteria to increase the measured 2D IR signal by enhancing the third-order signal with plasmon enhancement and decreasing the local oscillator intensity. By using an inverted reflection geometry, the method is not limited to the strict angle requirements of ATR IR spectroscopy. In fact, using an angle that is far from total internal reflection provides enhancement to the ΔOD. We also use an inverted reflection geometry on a solid/liquid interface. Specifically, a peptide monolayer is tethered to a $Au/CaF_2$ substrate and hydrated with $H_2O$, demonstrating the potential of SEAR 2D IR spectroscopy for more experiments in environments containing strongly absorbing solvents that were not previously possible. One such experiment includes developing 2D IR spectroscopy biological assays that require high sensitivity and low detection limits. The SEAR method could also be applied to the visible spectrum, creating SEAR 2D electronic spectroscopy (ES). While interfacial dynamics of charge carries in photovoltaic materials at electrodes are currently being investigated by other surface sensitive techniques, implementing SEAR 2D ES would make these measurements experimentally easier due to the enhanced signals observed. Moreover, the data collection with SEAR 2D IR spectroscopy is 5-10 times faster than our conventional transmission 2D IR experiments, making possible more difficult experiments, such as transient 2D IR spectroscopy. In general, SEAR 2D IR spectroscopy can be implemented in any 2D spectrometer, broadening the usefulness of multidimensional spectroscopy as an analytical tool as it can now be applied to monolayers and bulk systems of both gas and condensed phase samples.

## SUPPLEMENTARY MATERIAL

See supplementary material for details on predicted enhancement model, density functional theory (DFT) calculations, and other results.

## ACKNOWLEDGMENTS

Support for this research was funded by Grant Nos. NSF CHE 1665110, NIH GM 102387, NIH T32 GM008349, and NIH NIDDK 79895. E.R.B. is a trainee in UW-Madison's Biotechnology Training Program. J.P.L. is a Howard Hughes Medical Institute Fellow of the Life Sciences Research Foundation. M.T.Z. is a co-owner of PhaseTech Spectroscopy, Inc., which manufactures mid-IR pulse shapers and 2D IR spectrometers.

## REFERENCES

[1] F. Hoffmann, Surf. Sci. Rep. **3**, 107 (1983).
[2] W. G. Golden, D. S. Dunn, and J. Overend, J. Catal. **71**, 395 (1981).
[3] A. H. Martin, M. B. J. Meinders, M. A. Bos, M. A. Cohen Stuart, and T. van Vliet, Langmuir **19**, 2922 (2003).
[4] T. Buffeteau, B. Desbat, and J. M. Turlet, Appl. Spectrosc. **45**, 380 (1991).
[5] J. Fahrenfort, Spectrochim. Acta **17**, 698 (1961).
[6] C. Vigano, L. Manciu, F. Buyse, E. Goormaghtigh, and J.-M. Ruysschaert, Biopolymers **55**, 373 (2000).
[7] A. J. McQuillan, Adv. Mater. **13**, 1034 (2001).
[8] Y. R. Shen, Nature **337**, 519 (1989).
[9] H. Wang, E. C. Y. Yan, E. Borguet, and K. B. Eisenthal, Chem. Phys. Lett. **259**, 15 (1996).
[10] L. Fu, J. Liu, and E. C. Y. Yan, J. Am. Chem. Soc. **133**, 8094 (2011).
[11] F. M. Geiger, Annu. Rev. Phys. Chem. **60**, 61 (2009).
[12] I. V. Stiopkin, C. Weeraman, P. A. Pieniazek, F. Y. Shalhout, J. L. Skinner, and A. V. Benderskii, Nature **474**, 192 (2011).
[13] Z. Wang, J. A. Carter, A. Lagutchev, K. K. Yee, N. H. Seong, D. G. Cahilll, and D. D. Dlott, Science **317**, 787 (2007).
[14] J. P. Kraack and P. Hamm, Chem. Rev. **117**, 10623 (2017).
[15] J. Bredenbeck, A. Ghosh, H.-K. Nienhuys, and M. Bonn, Acc. Chem. Res. **42**, 1332 (2009).
[16] S. Nihonyanagi, S. Yamaguchi, and T. Tahara, Chem. Rev. **117**, 10665 (2017).
[17] P. Hamm and M. T. Zanni, *Concepts and Methods of 2D Infrared Spectroscopy* (Cambridge University Press, NY, 2011).
[18] S. Mukamel, *Principles of Nonlinear Optical Spectroscopy* (Oxford University Press, NY, 1995).
[19] M. Cho, *Two-Dimensional Optical Spectroscopy* (Taylor & Francis Group, Boca Raton, 2009).
[20] M. Khalil, N. Demirdöven, and A. Tokmakoff, J. Phys. Chem. A **107**, 5258 (2003).
[21] A. Ghosh, J. S. Ostrander, and M. T. Zanni, Chem. Rev. **117**, 10726 (2017).

[22]M. K. Petti, J. P. Lomont, M. Maj, and M. T. Zanni, J. Phys. Chem. B **122**, 1771 (2018).
[23]S.-H. Shim and M. T. Zanni, Phys. Chem. Chem. Phys. **11**, 748 (2008).
[24]P. M. Donaldson and P. Hamm, Angew. Chem., Int. Ed. **52**, 634 (2013).
[25]J. P. Kraack and P. Hamm, Phys. Chem. Chem. Phys. **18**, 16088 (2016).
[26]J. P. Kraack, A. Kaech, and P. Hamm, J. Phys. Chem. C **120**, 3350 (2016).
[27]Y. L. A. Rezus and O. Selig, Opt. Express **24**, 12202 (2016).
[28]O. Selig, R. Siffels, and Y. L. A. Rezus, Phys. Rev. Lett. **114**, 233004 (2015).
[29]R. T. Mackin, B. Cohn, A. Gandman, J. D. Leger, L. Chuntonov, and I. V. Rubtsov, J. Phys. Chem. C **122**, 11015 (2018).
[30]W. Xiong and M. T. Zanni, Opt. Lett. **33**, 1371 (2008).
[31]J. Réhault and J. Helbing, Opt. Express **20**, 21665 (2012).
[32]J. Nishida, C. Yan, and M. D. Fayer, J. Chem. Phys. **146**, 094201 (2017).
[33]C. Yan, J. E. Thomaz, Y.-L. Wang, J. Nishida, R. Yuan, J. P. Breen, and M. D. Fayer, J. Am. Chem. Soc. **139**, 16518 (2017).
[34]S.-H. Shim, D. B. Strasfeld, Y. L. Ling, and M. T. Zanni, Proc. Natl. Acad. Sci. U. S. A. **104**, 14197 (2007).
[35]C. T. Middleton, A. M. Woys, S. S. Mukherjee, and M. T. Zanni, Methods **52**, 12 (2010).
[36]L. E. Buchanan, E. B. Dunkelberger, H. Q. Tran, P.-N. N. Cheng, C.-C. C. Chiu, P. Cao, D. P. Raleigh, J. J. de Pablo, J. S. Nowick, and M. T. Zanni, Proc. Natl. Acad. Sci. U. S. A. **110**, 19285 (2013).
[37]T. R. Johnson, B. E. Mann, I. P. Teasdale, H. Adams, R. Foresti, C. J. Green, and R. Motterlini, Dalton Trans. **0**, 1500 (2007).
[38]T. Santos-Silva, A. Mukhopadhyay, J. D. Seixas, G. J. L. Bernardes, C. C. Romão, and M. J. Romão, J. Am. Chem. Soc. **133**, 1192 (2011).
[39]J. T. King, E. J. Arthur, C. L. Brooks, and K. J. Kubarych, J. Phys. Chem. B **116**, 5604 (2012).
[40]E. C. Fulmer, F. Ding, P. Mukherjee, and M. T. Zanni, Phys. Rev. Lett. **94**, 067402 (2005).
[41]J. E. Laaser, J. R. Christianson, T. A. Oudenhoven, Y. Joo, P. Gopalan, J. R. Schmidt, and M. T. Zanni, J. Phys. Chem. C **118**, 5854 (2014).
[42]T. A. Oudenhoven, Y. Joo, J. E. Laaser, P. Gopalan, and M. T. Zanni, J. Chem. Phys. **142**, 212449 (2015).
[43]D. E. Rosenfeld, Z. Gengelicki, B. J. Smith, T. D. P. Stack, and M. D. Fayer, Science **334**, 634 (2011).
[44]Z. Ganim, H. S. Chung, A. W. Smith, L. P. DeFlores, K. C. Jones, and A. Tokmakoff, Acc. Chem. Res. **41**, 432 (2008).
[45]Y. S. Kim and R. M. Hochstrasser, J. Phys. Chem. B **113**, 8231 (2009).
[46]M. V. Sawai, A. J. Waring, W. R. Kearney, P. B. McCray, W. R. Forsyth, R. I. Lehrer, and B. F. Tack, Protein Eng. **15**, 225 (2002).
[47]A. M. Woys, Y. S. Lin, A. S. Reddy, W. Xiong, J. J. De Pablo, J. L. Skinner, and M. T. Zanni, J. Am. Chem. Soc. **132**, 2832 (2010).
[48]B. Ding, J. E. Laaser, Y. Liu, P. Wang, M. T. Zanni, and Z. Chen, J. Phys. Chem. B **117**, 14625 (2013).
[49]S. Yamaguchi, D. Huster, A. Waring, R. I. Lehrer, W. Kearney, B. F. Tack, and M. Hong, Biophys. J. **81**, 2203 (2001).
[50]A. K. Nowinski, F. Sun, A. D. White, A. J. Keefe, and S. Jiang, J. Am. Chem. Soc. **134**, 6000 (2012).
[51]K. Kitagawa, T. Morita, and S. Kimura, J. Phys. Chem. B **108**, 15090 (2004).
[52]D. Enders, T. Nagao, A. Pucci, T. Nakayama, and M. Aono, Phys. Chem. Chem. Phys. **13**, 4935 (2011).
[53]T. La Cour Jansen and J. Knoester, J. Chem. Phys. **124**, 044502 (2006).
[54]T. La Cour Jansen, A. G. Dijkstra, T. M. Watson, J. D. Hirst, and J. Knoester, J. Chem. Phys. **125**, 044312 (2006).
[55]T. L. C. Jansen, J. Phys. Chem. B **118**, 8162 (2014).
[56]M. F. DeCamp, L. DeFlores, J. M. McCracken, A. Tokmakoff, K. Kwac, and M. Cho, J. Phys. Chem. B **109**, 11016 (2005).
[57]P. Roach, D. Farrar, and C. C. Perry, J. Am. Chem. Soc. **127**, 8168 (2005).
[58]M. Grechko and M. T. Zanni, J. Chem. Phys. **137**, 184202 (2012).
[59]E. B. Dunkelberger, M. Grechko, and M. T. Zanni, J. Phys. Chem. B **119**, 14065 (2015).
[60]J. P. Lomont, J. S. Ostrander, J.-J. Ho, M. K. Petti, and M. T. Zanni, J. Phys. Chem. B **121**, 8935 (2017).
[61]B. Cho, V. Tiwari, and D. M. Jonas, Anal. Chem. **85**, 5514 (2013).
[62]M. Osawa and K. Ataka, Surf. Sci. **262**, L118 (1992).
[63]Y. Nishikawa, T. Nagasawa, K. Fujiwara, and M. Osawa, Vib. Spectrosc. **6**, 43 (1993).
[64]M. Osawa, K.-I. Ataka, K. Yoshii, and Y. Nishikawa, Appl. Spectrosc. **47**, 1497 (1993).
[65]L. Chuntonov, R. Kumar, and D. G. Kuroda, Phys. Chem. Chem. Phys. **16**, 13172 (2014).
[66]W. L. Barnes, A. Dereux, and T. W. Ebbesen, Nature **424**, 824 (2003).
[67]A. V. Zayats and I. I. Smolyaninov, J. Opt. A: Pure Appl. Opt. **5**, S16 (2003).
[68]J. Zhang, L. Zhang, and W. Xu, J. Phys. D: Appl. Phys. **45**, 113001 (2012).
[69]S. Krimm and J. Bandekar, Adv. Protein Chem. **38**, 181 (1986).
[70]S. W. Englander and L. Mayne, Annu. Rev. Biophys. Biomol. Struct. **21**, 243 (1992).
[71]Y. Wu, K. Murayama, and Y. Ozaki, J. Phys. Chem. B **105**, 6251 (2001).
[72]A. Barth, Biochim. Biophys. Acta, Bioenerg. **1767**, 1073 (2007).